Ultrasmall Microlens Array Based on Vertically Aligned Carbon Nanofibers

Qing Dai, Ranjith Rajasekharan, Haider Butt, Xiaohui Qiu, Gehan Amaragtunga, and Timothy D. Wilkinson*

With the enhancement in performance of optical sensors and display systems, there is an increasing demand for ultrasmall microlenses (with dimensions less than 10 μm). Such lenses form high-resolution microlens arrays (MLAs), which are used for increasing the viewing angle of artificial compound-eye systems,[1,2] improving the quality of three-dimensional imaging systems,[3–5] and boosting the extraction efficiency of organic light-emitting diode (OLED) display panels.[6,7] In recent years, an enormous amount of research has been dedicated towards realizing such micrometer-scale lenses. Liquid microlenses with a high degree of tunability have been developed by several groups, but their sizes are generally several hundred micrometers.[8,9] Thus, they are not suitable for high-resolution display applications. Microlenses fabricated on optical plastic offer several micrometer diameters with low cost, but they suffer from larger thermal expansion and low glass transition temperatures.[10] Nanoscale lenses have also been reported recently with nanoscale diameters but the random patterns caused by self-assembly make them difficult to use.[11]

Our group has recently demonstrated a liquid-crystal (LC)-based reconfigurable microlens with diameter around 10 μm, which utilizes carbon nanofibers (CNFs) grown on a Si substrate as electrodes. Both simulation and experimental data have shown that this microlens has a focal length tunable via the control voltage.[12,13] However, the aperture of this microlens is irregular because of the nonuniform morphology of grown CNFs.

Herein, we demonstrate a newly designed microlens and report the detailed characterization of its optical properties. This work differs from previously reported microlenses, because here we utilize multiple CNFs as electrodes.[12,13] A single CNF was grown at the center of a dielectric circle to form a well-ordered lens aperture. This geometry suppresses the background electric field from the bottom electrode where the CNFs are grown, and thus the electric field from the CNF only is used for creating a refractive index profile to create the MLA. Additionally, the diameter of this microlens was decreased to 3 μm to increase the practicability, and it also has great potential to be reduced to 1 μm. Moreover, we also studied a highly reproducible recipe to fabricate patterned vertically aligned CNFs on metal electrodes.

A schematic diagram of the MLA is shown in **Figure 1**a. The 2D static electric field distribution around the CNFs was simulated using the finite element simulation method. The bottom electrode consisting of a CNF on a metal plate was placed at a potential of 5 V, while the top planar metal electrode was set to ground. A 4-μm-wide dielectric (electrically inactive) region was introduced around the CNF. The simulation result (Figure 1b) shows that due to the presence of a dielectric region around the CNF, a uniform Gaussian-like electric field profile was generated. The advantage of this geometry is that the electric field profile, in the dielectric region around the CNFs, is only defined by the CNFs. Therefore, the alignment of the LC molecules and consequently the aperture of each lenslet would be uniform even when the fabricated CNFs are inconsistently grown.

Based on the simulation results the fabrication of a CNF array was performed. A silicon dioxide substrate covered with tungsten electrode was patterned by photolithography with 500-nm-wide mesh lines. The exposed circles, with a diameter of the order of 3 μm representing the dielectric regions, were composed of silicon dioxide. A vertically aligned CNF was grown at the center by using plasma-enhanced chemical vapor deposition (PECVD).[14] Electron-beam lithography and lift-off were employed to produce an array of Al (10 nm)/Ni (7 nm) multilayer catalyst dots 100 nm in diameter. The sample was heated to 720 °C on a graphite stage, while ammonia gas (200 sccm) was introduced to anneal the catalyst for 60 s. After that, the plasma was ignited by applying a dc voltage (640 V) between the grounded stage and the shower head with an NH_3/C_2H_2 (200/50 sccm) gas mixture pumped in at a pressure of 3.1 mbar. This growth process lasted for 25–30 min, while synthesizing CNFs nearly 5 μm in height. The growth direction of CNFs was determined by

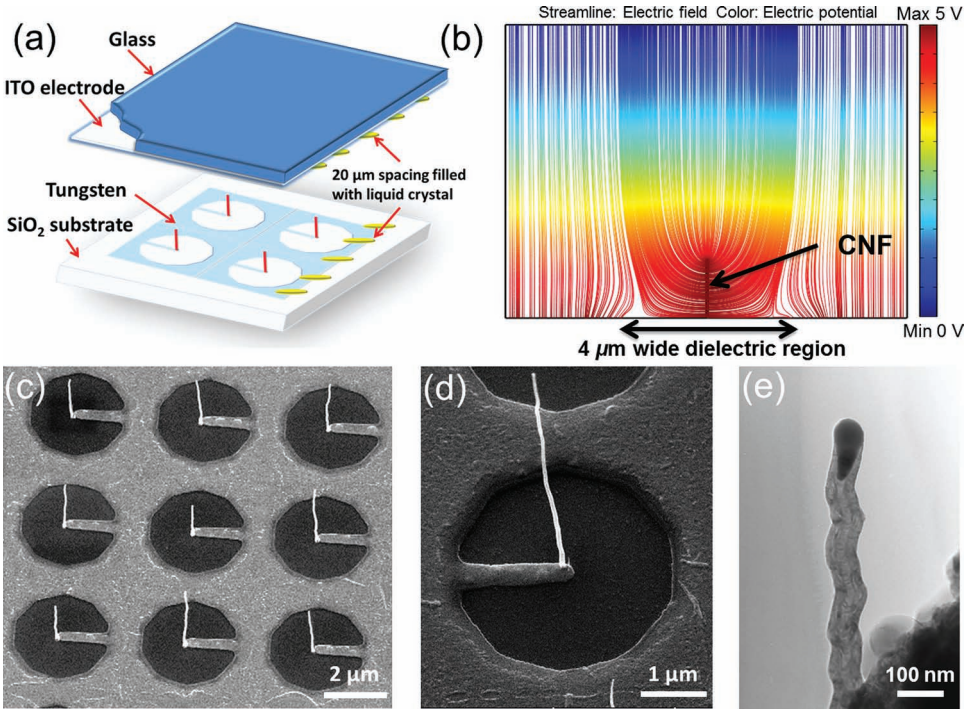

Figure 1. a) Schematic diagram of the MLA. b) Simulation results of the electric field distribution along the cross section of the MLA. c) SEM image of the grown CNF electrodes. d) Zoomed-in image of a single aperture. e) TEM image of a multiwalled CNF with diameter around 85 nm.

the reaction gas flow. In our growth process, acetylene and ammonia were injected perpendicularly to the surface of substrates by the gas shower. Moreover, the dc plasma also made a contribution towards the vertical growth of CNFs, as a vertical electric field was generated between the gas shower and substrate. Figure 1c and d display the scanning electron microscopy (SEM) images of the fabricated electrodes at a 30° tilt. Uniform and vertically aligned CNFs were fabricated at the center of dielectric circles as control electrodes and each dielectric circle was fabricated with same dimension for uniform apertures. Transmission electron microscopy (TEM) measurement indicates the multiwalled structure of the grown CNFs with diameter around 85 nm as shown in Figure 1e.

The CNF array was then assembled with a top electrode consisting of a layer of indium tin oxide (ITO) on 0.5-mm-thick borosilicate glass, to form a cell. The top electrode was also given a planar alignment for LCs by spin-coating and rubbing a thin film of polyimide (AM4276, Merck). Due to the planar alignment the LC molecules acquired a horizontal orientation at 0 V in the bulk of the device. On application of potential the LC molecules rotated parallel to the vertical electric fields produced between the electrodes. A horizontal alignment in the off-state (0 V) allowed a good optical contact for measuring the lensing behavior. A 20 μm cell gap between substrates was set by silica spacer beads in UV-curing adhesive, and the cell was then filled with a nematic LC (BL048, Merck). **Figure 2**a shows the fabricated lens array switching at 1.2 Vrms under an optical microscope with an objective magnification of ×60. Uniform circular lenslets were observed under the microscope, which shows the vertical alignment of CNFs was not affected by the LC filling process.

The real modulation capability and practicability of this MLA device greatly depend on the microscopic phase profile of each lenslet. This phase profile was obtained from

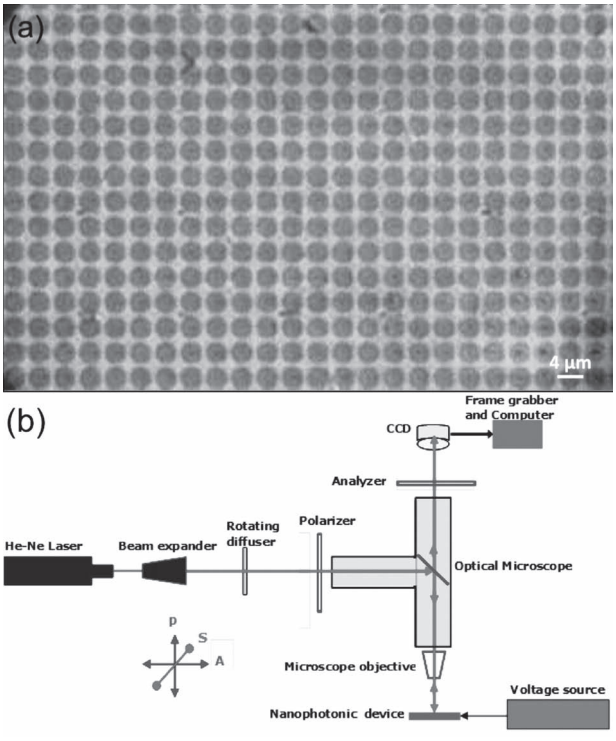

Figure 2. a) Lens array switching at 1.2 Vrms under an optical microscope (magnification ×60). b) Experimental setup for recording interference fringes from the lens array in reflective mode.

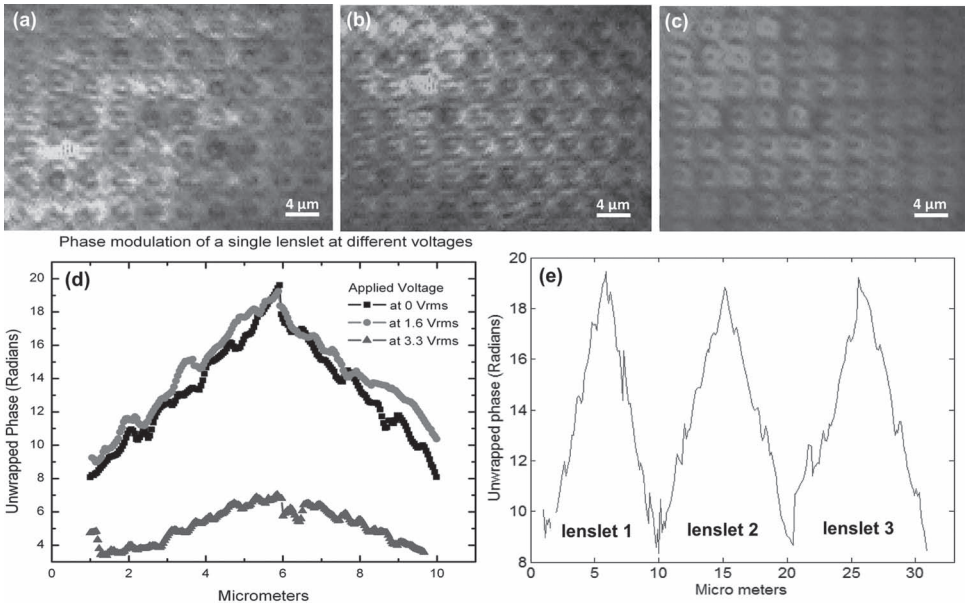

Figure 3. Interference fringes of the lens array working at different voltages: a) 0, b) 1.6, and c) 3.3 Vrms. d) Phase modulation of a single lenslet at different voltages: 0, 1.6, and 3.3 Vrms. The maximum phase modulation observed was around 3.8π. e) Phase modulation of three lenslets at 1.4 Vrms.

interference fringes followed by phase recovery using Fourier transform techniques.[13] The interference setup consisted of a He–Ne laser along with a beam expander as the illuminating source, as shown in Figure 2b. An objective having a magnification of ×60 was used in the microscope to illuminate the selected area and also to receive the reflected beam. The lens array was mounted on a fine three-axis tilting stage in the microscope. The rubbing direction of the lens array was kept at 45° to the polarizer. The interference fringes were formed due to the interference between the ordinary and extraordinary beams being combined by an analyzer which was crossed with the polarizer.[15] A rotating diffuser (transparent plastic sheet) was used to average out speckle noise. The fringes were recorded on a CCD camera and frame grabber.

Figure 3a–c shows the interference fringes from the lens array at 0, 1.6, and 3.3 Vrms. We studied the distribution of change in phase modulation of each lenslet at different voltages. In the absence of an external voltage circular fringes were observed, which confirms an alignment deformation of the LC molecules near the CNF even though the macroscopic alignment was planar on the top electrode. The phase modulations of a lenslet were calculated as 3.9, 3.2, and 1.1π at 0, 1.9, and 3.3 Vrms, respectively, as shown in Figure 3d. Although the lenslets were fabricated for a diameter near 3 μm, the LC director profile around the CNFs extended to approximately 10 μm. This is because the phase profiles recorded were not the actual ones from the microlens, but were projections of the genuine phase profiles on the bottom of the top glass substrate. Due to the lensing effect caused by aligned LC molecules, these projected phase profiles were magnified as their locations were moved away from the bottom substrate. We also calculated the phase profile of an array of three lenslets at a fixed voltage to prove the device performance, as shown in Figure 3e. The noise in the phase profile is mainly due to the noise from the unwrapping algorithm used. The low contrast in the recorded fringes was due to low reflection from the silicon dioxide where the CNF is grown and limitation in CCD resolution in capturing the fringes from a few-micrometer region. Though the lenslets were designed for a diameter of 3 μm, the fringes occupied more than this area. A slight variation in the phase modulation was observed in different focal planes due to the hybrid alignment of the device across the thickness. We measured the reflectivity of the lens array as 30% at 0 Vrms. The reflectivity of the lens array varied with respect to the applied voltage and was found to have a maximum value of 40% at 7 Vrms.

The maximum phase modulation measured was around 4π. The interference fringes were further used to characterize the focal length of each lenslet in the array. We calculated the focal length of the lenslet from the phase profile using the equation $f = \frac{r^2}{2\lambda N}$,[16] where r is the diameter of the lenslet, N is the number of observed fringes, and λ is the wavelength of light (633 nm). The focal length varied from 6 μm at 0 Vrms to 12 μm at 3.3 Vrms. However, the higher focal length region (12 μm region) was not useful for lens array applications because of the distortion in the LC at each lenslet profile at higher voltages. The focal length variation was very small with respect to the applied voltage because of the very small size of the lenslet. Larger focal lengths are possible by increasing the refractive index across the lenslet by applying different voltages to the CNFs and surrounding electrodes.

In conclusion, a 3-μm-diameter lens array was fabricated using nematic LCs and CNFs. The fabricated array was uniform with around 10^6 lenslets in a 10 mm × 10 mm area. In the lens array, each lenslet was formed around the CNF. The silicon dioxide dielectric material under the nanofibers suppressed the background electric field from the bottom

substrate, and gave a more Gaussian electric field profile and hence more uniformity in the lens array switching. The very small focal length of the device finds application in near-field imaging, fine sampling of an object under consideration in integral imaging microscopy, and for uniform illumination in display panels.

Acknowledgements

This work was partly funded under the Nokia–Cambridge Strategic Partnership in Nanoscience and Nanotechnology (Energy Program).

[1] K. H. Jeong, J. Kim, L. P. Lee, *Science* **2006**, *312*, 557.
[2] J. Duparre, P. Dannberg, P. Schreiber, A. Brauer, A. Tunnermann, *Appl. Optics* **2005**, *44*, 2949.
[3] R. Martinez-Cuenca, A. Pons, G. Saavedra, M. Martinez-Corral, B. Javidi, *Opt. Express* **2006**, *14*, 9657.
[4] J. Arai, F. Okano, H. Hoshino, I. Yuyama, *Appl. Optics* **1998**, *37*, 2034.
[5] R. Rajasekharan, T. D. Wilkinson, P. J. W. Hands, Q. Dai, *Nano Lett.* **2011**, *11*, 2770.
[6] H. W. Choi, C. Liu, E. Gu, G. McConnell, J. M. Girkin, I. M. Watson, M. D. Dawson, *Appl. Phys. Lett.* **2004**, *84*, 2253.
[7] J. P. Yang, Q. Y. Bao, Z. Q. Xu, Y. Q. Li, J. X. Tang, S. Shen, *Appl. Phys. Lett.* **2010**, *97*, 3.
[8] U. Levy, R. Shamai, *Microfluid. Nanofluid.* **2008**, *4*, 97.
[9] T. Krupenkin, S. Yang, P. Mach, *Appl. Phys. Lett.* **2003**, *82*, 316.
[10] H. Ottevaere, R. Cox, H. P. Herzig, T. Miyashita, K. Naessens, M. Taghizadeh, R. Volkel, H. J. Woo, H. Thienpont, *J. Opt. A: Pure Appl. Opt.* **2006**, *8*, S407.
[11] J. Y. Lee, B. H. Hong, W. Y. Kim, S. K. Min, Y. Kim, M. V. Jouravlev, R. Bose, K. S. Kim, I. C. Hwang, L. J. Kaufman, C. W. Wong, P. Kim, *Nature* **2009**, *460*, 498.
[12] T. D. Wilkinson, X. Wang, K. B. K. Teo, W. I. Milne, *Adv. Mater.* **2008**, *20*, 363.
[13] Q. Dai, R. Rajasekharan, H. Butt, K. Won, X. Wang, T. Wilkinson, G. Amaragtunga, *Nanotechnology* **2011**, *22*, 115201.
[14] K. Teo, M. Chhowalla, G. Amaratunga, W. Milne, G. Pirio, P. Legagneux, F. Wyczisk, D. Pribat, D. Hasko, *Appl. Phys. Lett.* **2002**, *80*, 2011.
[15] T. Amemiya, H. Shimizu, Y. Nakano, P. Hai, M. Yokoyama, M. Tanaka, *Appl. Phys. Lett.* **2006**, *89*, 021104.
[16] R. Rajasekharan, C. Bay, Q. Dai, J. Freeman, T. Wilkinson, *Appl. Phys. Lett.* **2010**, *96*, 233108.